, AND C. SPALTER, *Amer. J. Roentgenol.*
:R, J. WATTS, AND M. ARAKAWA, *Magn.*
R. T. GO, Y. NOSE, AND T. F. MEANEY,
687 (1985).
Phys. **14,** 43 (1987).
.. Thomas and A. Margulis, Eds.), Chap.
ıdation, San Francisco, 1984.
63, 784 (1987).
983 (1987).
111-117. CRC Press, Boca Raton, FL,
w Dynamics and Measurements," Chap.
ıkabo Press, Tokyo, 1973.
is **55,** 415 (1986).
:. MALLOY, AND R. W. PARKEY, *Magn.*
ERNSTEIN, *J. Comput. Assisted Tomogr.*
597. Cambridge Univ. Press, Cambridge,
'eson. Med. **3,** 303 (1986).
).

MAGNETIC RESONANCE IN MEDICINE **15,** 287–304 (1990)

Simultaneous Spatial and Spectral Selective Excitation

CRAIG H. MEYER, JOHN M. PAULY, ALBERT MACOVSKI, AND DWIGHT G. NISHIMURA

Information Systems Laboratory, Stanford University, Stanford, California 94305

Received January 17, 1989; revised December 29, 1989

Using a **k**-space interpretation of small-tip excitation, a single excitation pulse has been designed that is simultaneously selective in space and resonant frequency. An analytic expression for the response of this pulse has been derived. The pulse has been implemented on a 1.5-T imaging system. The pulse has been applied to a rapid gradient–echo imaging sequence that forms both water and fat images within a breath-holding interval. These rapid images are free of the chemical shift artifacts at organ boundaries that typically afflict conventional rapid images. The pulse can be applied to a variety of other sequences, such as multislice water/fat sequences and rapid **k**-space scanning sequences.

INTRODUCTION

For a number of imaging applications one would like to selectively examine a particular spatial slice and a particular spectral component of the object at the same time. The most important example of this is two-dimensional water/fat imaging. Water/fat imaging may be desirable as an end in itself, for example, as a tool for examining atherosclerotic plaque. It may also be desirable to select for water or fat to avoid image artifacts, such as those encountered in rapid imaging sequences. Rapid gradient–echo imaging sequences based on steady-state free precession, such as FLASH (*1*), GRASS (*2*), FFE (*3*), FAST (*4*), and SSFP (*5*), suffer from artifacts at water/fat boundaries. Rapid **k**-space scanning sequences can suffer intolerable shifts or blurring of either water or fat (*6–8*).

Many techniques for forming water/fat images using spectrally selective excitation sequences have been studied. Most of these techniques combine a spatially selective pulse with an additional spectrally selective pulse (*9, 10*); multislice acquisition is impossible with these techniques. One recent technique uses two offset spatially selective pulses (*11, 12*). However, for many applications a single pulse that is simultaneously spectrally selective and spatially selective is preferable to a combination of pulses. Using the **k**-space interpretation of small-tip excitation introduced by Pauly *et al.* (*13*), we have designed such a pulse (*14, 15*). We will refer to this kind of pulse as a spatial–spectral pulse.

In this paper we first review excitation **k** space. Then we derive theoretical expressions for the magnetization excited in the presence of oscillating gradients. Next we discuss the design of a spatial–spectral pulse for water/fat imaging. We present computer simulations and experimental results that verify the theory. We apply the pulse

0740-3194/90 $3.00

to a rapid gradient–echo sequence and obtain water/fat images of a normal volunte at 1.5 T. Finally, we discuss some of the issues, advantages, disadvantages, and app cations of simultaneous spatial and spectral selective excitation.

EXCITATION k SPACE

Pauly *et al.* (*13*) introduced a **k**-space interpretation of small-tip-angle selecti excitation. They showed that multidimensional selective excitation in the presen of time-varying gradients can be analyzed using Fourier transform theory. Using tl interpretation, they designed and implemented selective excitation pulses that selective in two spatial dimensions. This **k**-space interpretation of excitation provid many of the same conceptual advantages as the well-known **k**-space interpretati of the readout mode of magnetic resonance imaging (MRI) (*16–20*), although differs in some important respects.

We first summarize the **k**-space interpretation of selective excitation by reviewi some results from (*13*). Using the well-known small-tip-angle approximation, t Bloch equation can be solved to give the following expression for the transverse ma netization:

$$M_{xy}(\mathbf{r}) = i\gamma M_0(\mathbf{r}) \int_{\mathbf{K}} W(\mathbf{k})S(\mathbf{k})e^{i\mathbf{r}\cdot\mathbf{k}}d\mathbf{k},$$

where

$$W(\mathbf{k}(t)) = \frac{B_1(t)}{|\dot{\mathbf{k}}(t)|}$$

$$S(\mathbf{k}) = \int_0^T \{\delta(\mathbf{k}(t) - \mathbf{k})|\dot{\mathbf{k}}(t)|\}\, dt.$$

We will define the relevant **k**-space variables shortly. $W(\mathbf{k})$ is a weighting functi in multidimensional **k** space. $S(\mathbf{k})$ is a sampling grid in **k**-space. The factor $|\dot{\mathbf{k}}($ normalizes $S(\mathbf{k})$ so that it is a unit-strength line delta. A unit-strength line delta defined as a line delta that integrates to unity along a unit-length path. The transve magnetization excited is proportional to the product of the initial magnetization a the inverse Fourier transform of the product of $W(\mathbf{k})$ and $S(\mathbf{k})$. In designing excitation pulse having a given spatial distribution and its associated transform, o first chooses a **k** trajectory such that $S(\mathbf{k})$ provides an adequate **k**-space samplin grid. Then one can choose $W(\mathbf{k})$ as the Fourier transform of the main lobe of th desired transverse magnetization, within the limits of the small-tip approximatio Once $S(\mathbf{k})$ and $W(\mathbf{k})$ are chosen, it is straightforward to determine the correspondin gradient and RF waveforms.

The problem of designing a pulse that is spatially and spectrally selective is simila to the problem of designing a pulse that is selective in two spatial dimensions (*13*) We wish to design a pulse that is selective in both the slice-selection direction, z, an the spectral direction, ω. We thus define **k**-space axes corresponding to z and ω a follows:

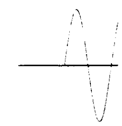

FIG. 1. Excitation **k**-space trajectory fo The trajectory ends at the origin.

$$k_z(t) = -R$$

Note that the integration defini in contrast to readout **k** space, interval up to the observation ti

The constant R in Eq. [4] is a c problems. To design a pulse in the gyromagnetic ratio. In that units of distance. In our problen different. We choose the units o This means that the numerical v choosing a relation between the might choose the value of R late normalization factor, $|\dot{\mathbf{k}}(t)|$, in ing magnetization. When one i convert k_z back to natural units

Because the **k** trajectory is c axis, one must oscillate the slice- structure in (k_z, k_ω) space. Vari discussion will center upon sinu

$$G_z(t) = ($$

This $G_z(t)$ corresponds to the f

$$k_z = \frac{RG}{\Omega} \sin \Omega(t$$

This **k** trajectory is shown in Fi space, it ends at the origin, as a

In this section, we derive the pulse. The results of this deriv spectral pulses. The technique

ater / fat images of a normal volunteer
advantages, disadvantages, and appli-
ective excitation.

SPACE

pretation of small-tip-angle selective
l selective excitation in the presence
Fourier transform theory. Using this
l selective excitation pulses that are
interpretation of excitation provides
e well-known **k**-space interpretation
naging (MRI) (*16–20*), although it

ı of selective excitation by reviewing
small-tip-angle approximation, the
ıg expression for the transverse mag-

$)S(\mathbf{k})e^{i\mathbf{r}\cdot\mathbf{k}}d\mathbf{k},$ [1]

$t)$ / $)|$ [2]

$|\dot{\mathbf{k}}(t)|\}dt.$ [3]

rtly. $W(\mathbf{k})$ is a weighting function
grid in **k**-space. The factor $|\dot{\mathbf{k}}(t)|$
delta. A unit-strength line delta is
g a unit-length path. The transverse
ıct of the initial magnetization and
$W(\mathbf{k})$ and $S(\mathbf{k})$. In designing an
ı and its associated transform, one
des an adequate **k**-space sampling
transform of the main lobe of the
ts of the small-tip approximation.
ırd to determine the corresponding

y and spectrally selective is similar
e in two spatial dimensions (*13*).
he slice-selection direction, z, and
axes corresponding to z and ω as

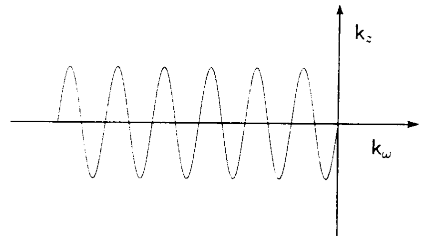

FIG. 1. Excitation **k**-space trajectory for a spatial–spectral pulse with a sinusoidal slice-selection gradient. The trajectory ends at the origin.

$$k_z(t) = -R\int_t^T G_z(s)ds \qquad k_\omega(t) = t - T. \qquad [4]$$

Note that the integration defining k_z ranges over the time remaining in the interval, in contrast to readout **k** space, where the integration ranges from the start of the interval up to the observation time.

The constant R in Eq. [4] is a constant that is defined differently for different design problems. To design a pulse in two spatial dimensions, we would set R equal to γ, the gyromagnetic ratio. In that case the units of k_z would be the reciprocal of the units of distance. In our problem, we have two **k**-space axes whose natural units are different. We choose the units of R so that k_z has the same units as k_ω, e.g., seconds. This means that the numerical value that we choose for R is arbitrary; we are in effect choosing a relation between the natural units of the axes. We will discuss how one might choose the value of R later. In the design of a pulse, R is used to compute the normalization factor, $|\dot{\mathbf{k}}(t)|$, in Eqs. [2] and [3], and it is used to calculate the resulting magnetization. When one is just interested in the spatial slice width, one can convert k_z back to natural units by setting $R = \gamma$.

Because the **k** trajectory is constrained to move linearly with time along the k_ω axis, one must oscillate the slice-selection gradient to generate an adequate sampling structure in (k_z, k_ω) space. Various forms of oscillation could be used. Most of our discussion will center upon sinusoidal oscillation of the form

$$G_z(t) = G\cos\Omega(t - T), \qquad 0 \leqslant t \leqslant T. \qquad [5]$$

This $G_z(t)$ corresponds to the following **k** trajectory:

$$k_z = \frac{RG}{\Omega}\sin\Omega(t - T) = \frac{RG}{\Omega}\sin\Omega k_\omega, \qquad -T \leqslant k_\omega \leqslant 0. \qquad [6]$$

This **k** trajectory is shown in Fig. 1. Rather than starting at the origin as in readout **k** space, it ends at the origin, as a consequence of Eq. [4].

THEORY

In this section, we derive the theoretical magnetization excited by a spatial–spectral pulse. The results of this derivation will help us in designing and applying spatial–spectral pulses. The techniques used in the derivation may be useful to the reader interested in the effects of applying an RF pulse in the presence of an oscillating gradient. The reader who is interested primarily in using spatial–spectral pulses can proceed to the following section without loss of continuity.

Using the small-tip-angle approximation, we will now calculate the magnetization excited by a spatial–spectral pulse having a sinusoidal slice-selection gradient. This magnetization is proportional to the product of $M_0(\omega, z)$ and the two-dimensional (2D) inverse Fourier transform of the product of $S(\mathbf{k})$ and $W(\mathbf{k})$.

Let us define the one-dimensional (1D) Fourier transform and its inverse as

$$F(u) = \int_{-\infty}^{\infty} f(x)e^{-iux}dx \qquad f(x) = \frac{1}{2\pi}\int_{-\infty}^{\infty} F(u)e^{iux}du. \qquad [7]$$

We designate 1D forward and inverse transforms by $\mathcal{F}\{\ \}$ and $\mathcal{F}^{-1}\{\ \}$, respectively, and their 2D counterparts by ${}^{2}\mathcal{F}\{\ \}$ and ${}^{2}\mathcal{F}^{-1}\{\ \}$. We use $*$ to represent 1D convolution and $**$ to represent 2D convolution. We define the rectangle function such that $\mathrm{rect}(x) = 1$ for $|x| < \frac{1}{2}$.

First we study the inverse Fourier transform of the unit-strength sinusoidal line delta, $S(\mathbf{k})$. We define the delta as

$$S(\mathbf{k}) = \sqrt{R^2G^2\cos^2\Omega k_\omega + 1}\,\delta\!\left(k_z - \frac{RG}{\Omega}\sin\Omega k_\omega\right). \qquad [8]$$

Let $S(\mathbf{k})$ extend over the infinite interval $-\infty < k_\omega < \infty$. Any realizable $S(\mathbf{k})$ will of course be of finite extent along the k_ω axis; we will account for this in $W(\mathbf{k})$. $S(\mathbf{k})$ is periodic along the k_ω axis with period $2\pi/\Omega$. We can decompose it into a 1D Fourier series with k_z as a parameter (*21*). We calculate the series coefficients, C_n, as

$$C_n(k_z) = \frac{\Omega}{2\pi}\int_{-\pi/\Omega}^{\pi/\Omega} \sqrt{R^2G^2\cos^2\Omega k_\omega + 1}\,\delta\!\left(k_z - \frac{RG}{\Omega}\sin\Omega k_\omega\right)e^{in\Omega k_\omega}dk_\omega. \qquad [9]$$

We want to express the argument of the delta function in the form $k_\omega - f(k_z)$, which involves inverting the sin function. Because $\sin^{-1}$ is a multivalued function, we must decompose this integral into four subintegrals, each ranging over a quarter of a cycle of $\sin\Omega k_\omega$. The first subintegral is

$$\frac{\Omega}{2\pi}\int_{-\pi/\Omega}^{-\pi/2\Omega} S(k_z, k_\omega)e^{in\Omega k_\omega}dk_\omega$$

$$= \int_{-\pi/\Omega}^{-\pi/2\Omega} \beta(k_z)\delta\left\{k_\omega - \left[-\frac{\pi}{\Omega} - \frac{1}{\Omega}\sin^{-1}\left(\frac{\Omega}{RG}k_z\right)\right]\right\}e^{in\Omega k_\omega}dk_\omega \qquad [10]$$

$$= \beta(k_z)e^{-in\pi}e^{-in\sin^{-1}(\Omega/RG)k_z)}, \qquad [11]$$

where

$$\beta(k_z) = \frac{\Omega}{2\pi}\frac{\sqrt{1 - \left(\frac{\Omega k_z}{RG}\right)^2 + \frac{1}{R^2G^2}}}{\sqrt{1 - \left(\frac{\Omega k_z}{RG}\right)^2}} = A\frac{\Omega}{2\pi}\frac{\sqrt{1 - \left(\frac{\Omega k_z}{ARG}\right)^2}}{\sqrt{1 - \left(\frac{\Omega k_z}{RG}\right)^2}} \qquad [12]$$

in the presence of an oscillating
using spatial–spectral pulses can
tinuity.

now calculate the magnetization
idal slice-selection gradient. This
$_0(\omega, z)$ and the two-dimensional
$\mathbf{k}$) and $W(\mathbf{k})$.
ransform and its inverse as

$$\frac{1}{2\pi}\int_{-\infty}^{\infty} F(u)e^{iux}du. \quad [7]$$

by $\mathcal{F}\{\ \}$ and $\mathcal{F}^{-1}\{\ \}$, respec-
$^{-1}\{\ \}$. We use $*$ to represent 1D
We define the rectangle function

the unit-strength sinusoidal line

$$\frac{RG}{\Omega}\sin\Omega k_\omega\Big). \quad [8]$$

$< \infty$. Any realizable $S(\mathbf{k})$ will of
ccount for this in $W(\mathbf{k})$. $S(\mathbf{k})$ is
decompose it into a 1D Fourier
series coefficients, C_n, as

$$-\frac{RG}{\Omega}\sin\Omega k_\omega\Big)e^{in\Omega k_\omega}dk_\omega. \quad [9]$$

nction in the form $k_\omega - f(k_z)$,
$\sin^{-1}$ is a multivalued function,
als, each ranging over a quarter

$$\mathrm{n}^{-1}\left(\frac{\Omega}{RG}k_z\right)\Bigg]\Bigg\}e^{in\Omega k_\omega}dk_\omega \quad [10]$$

[11]

$$\frac{2}{\pi}\frac{\sqrt{1-\left(\frac{\Omega k_z}{ARG}\right)^2}}{\sqrt{1-\left(\frac{\Omega k_z}{RG}\right)^2}} \quad [12]$$

TABLE 1

Fourier Series Coefficient Subintegrals

Limits	Argument of δ( )	Result	Range of k_z
$-\frac{\pi}{\Omega}$ to $-\frac{\pi}{2\Omega}$	$k_\omega + \frac{\pi}{\Omega} + \frac{1}{\Omega}\sin^{-1}\left(\frac{\Omega}{RG}k_z\right)$	$\beta(k_z)e^{-in\pi}e^{-in\sin^{-1}((\Omega/RG)k_z)}$	$-\frac{RG}{\Omega} \leqslant k_z < 0$
$-\frac{\pi}{2\Omega}$ to 0	$k_\omega - \frac{1}{\Omega}\sin^{-1}\left(\frac{\Omega}{RG}k_z\right)$	$\beta(k_z)e^{in\sin^{-1}((\Omega/RG)k_z)}$	$-\frac{RG}{\Omega} \leqslant k_z < 0$
0 to $\frac{\pi}{2\Omega}$	$k_\omega - \frac{1}{\Omega}\sin^{-1}\left(\frac{\Omega}{RG}k_z\right)$	$\beta(k_z)e^{in\sin^{-1}((\Omega/RG)k_z)}$	$0 \leqslant k_z \leqslant \frac{RG}{\Omega}$
$\frac{\pi}{2\Omega}$ to $\frac{\pi}{\Omega}$	$k_\omega - \frac{\pi}{\Omega} + \frac{1}{\Omega}\sin^{-1}\left(\frac{\Omega}{RG}k_z\right)$	$\beta(k_z)e^{in\pi}e^{-in\sin^{-1}((\Omega/RG)k_z)}$	$0 \leqslant k_z \leqslant \frac{RG}{\Omega}$

and

$$A = \sqrt{1 + \frac{1}{R^2G^2}}. \quad [13]$$

In Eq. [10] we have replaced the unit delta function of Eqs. [8] and [9] with a unit delta function that is equivalent within the limits of integration. For the remaining subintegrals the form of the equivalent unit delta function is slightly different; the argument of the delta varies, although the normalization factor remains the same. Table 1 summarizes the results for the four subintegrals. Each integral is valid for a particular range of k_z. We add the integrals in each k_z range to determine the following Fourier series coefficients:

$$C_n(k_z) = \begin{cases} \beta(k_z)2\,\mathrm{rect}\left(\frac{\Omega k_z}{2RG}\right)\cos\left[n\sin^{-1}\left(\frac{\Omega k_z}{RG}\right)\right] & \text{for } n \text{ even} \\ \beta(k_z)2i\,\mathrm{rect}\left(\frac{\Omega k_z}{2RG}\right)\sin\left[n\sin^{-1}\left(\frac{\Omega k_z}{RG}\right)\right] & \text{for } n \text{ odd.} \end{cases} \quad [14]$$

Substituting Eq. [12] into Eq. [14] and performing an inverse Fourier transform yield

$$\mathcal{F}^{-1}\{C_n(k_z)\} = K_1\frac{J_1(Az')}{2Az'} * J_n(z'), \quad [15]$$

where K_1 is a constant and

$$z' = \frac{RGz}{\Omega}. \quad [16]$$

The Fourier series for $S(\mathbf{k})$ is

$$S(k_z, k_\omega) = \sum_{n=-\infty}^{\infty} C_n(k_z)e^{-ink_\omega\Omega}. \quad [17]$$

The inverse Fourier transform of this series representation of $S(\mathbf{k})$ is

$$
\begin{aligned}
{}^2\mathcal{F}^{-1}\{S(k_\omega, k_z)\} &= \sum_{n=-\infty}^{\infty} \mathcal{F}^{-1}\{C_n(k_z)\}\delta(\omega - n\Omega) \\
&= K_1 \frac{J_1(Az')}{2Az'} * \sum_{n=-\infty}^{\infty} J_n(z')\delta(\omega - n\Omega).
\end{aligned} \qquad [18]
$$

The transform of $S(\mathbf{k})$ is thus a series of weighted line deltas parallel to the k_z axis and separated by Ω, the gradient modulation frequency.

Assuming $W(k_z, k_\omega) = W(k_z)W(k_\omega)$, the resulting transverse magnetization excited by the pulse is

$$
\begin{aligned}
M_{xy}(z, \omega) &= i2\pi\gamma M_0(z, \omega)\mathcal{F}^{-1}\{W(k_\omega)\} \\
&\times \delta(k_z) ** \sum_{n=-\infty}^{\infty} \mathcal{F}^{-1}\{C_n(k_z)W(k_z)\}\delta(\omega - n\Omega).
\end{aligned} \qquad [19]
$$

Combining Eq. [19] with Eq. [15] yields

$$
\begin{aligned}
M_{xy}(z, \omega) &= K_2 M_0(z, \omega)\mathcal{F}^{-1}\{W(k_\omega)\} \\
&\times \delta(k_z) ** \sum_{n=-\infty}^{\infty} \left[\mathcal{F}^{-1}\{W(k_z)\} * \frac{J_1(Az')}{2Az'} * J_n(z')\right]\delta(\omega - n\Omega),
\end{aligned} \qquad [20]
$$

where K_2 is a constant. This result shows that the nth sidelobe has the form of a smoothed J_n in the z direction and the form of the inverse transform of $W(k_\omega)$ in the ω direction. Assuming that the spacing of the spectral islands, Ω, is large compared to the width of $\mathcal{F}^{-1}\{W(k_\omega)\}$, Eq. [20] permits straightforward calculation of M_{xy} for separable W.

One can also calculate M_{xy} by looking at the solution of the Bloch equation in the time domain. This solution can be written as (*13, 22*)

$$
M_{xy}(z, \omega) = i\gamma M_0(z, \omega) \int_0^T B_1(t) e^{i(\gamma Gz/\Omega)\sin\Omega(t-T)} e^{i\omega(t-T)} dt. \qquad [21]
$$

Using the identity

$$
e^{i\alpha\sin\Omega t} = \sum_{n=-\infty}^{\infty} J_n(\alpha) e^{in\Omega t}, \qquad [22]
$$

we can rewrite Eq. [21] as

$$
M_{xy}(z, \omega) = i\gamma M_0(z, \omega) \sum_{n=-\infty}^{\infty} J_n\left(\frac{\gamma Gz}{\Omega}\right) \int_0^T B_1(t) e^{i(n\Omega+\omega)(t-T)} dt. \qquad [23]
$$

Here we also arrive at an infinite sum containing J_n. This equation can be used to calculate M_{xy}, although Eq. [20] is more practical for most purposes. To approximately calculate the sidelobe at $\omega = k\Omega$, the infinite sum in Eq. [23] can be replaced by a finite sum centered at $n = -k$. The number of terms required depends upon how rapidly $B_1(t)$ varies.

To this point we have assum
dal fashion. This is a convenien
experiments and simulations h
we can also calculate the mag
employed. The derivation is sir
the result here.

Assume that $G_z(t)$ is a squa
magnetization can then be expr

$M_{xy}(z, \omega) = K_3 M_0(z, \omega)\mathcal{F}^{-1}\{$

$\times\ \delta$

where K_3 is a constant and

$a_n(z) = \{$ sinc(... sinc(

In this equation sinc $(x) = ($sin

DI

We now have expressions fo
of an oscillating slice-selection
design of pulses that are simul
Some of the considerations in
of the slice-selection gradient,
of the desired and undesired co
amplitude and frequency of th
the RF envelope, which detern
spectral slice profiles, (5) the l
pulses to shift them in space and
tions in the context of the desig

We wish to design a slice-sel
nates against fat protons, or vi
difference frequency between w
field inhomogeneity across the
The main requirement for th
in some manner so that the k
arguments, it makes intuitive s
G_z. We know that any long R
gradients. We want to add a G_z
prevent chemical shift from sir
tion is to oscillate the gradient.
of slew-rate limitations. Here

ntation of $S(\mathbf{k})$ is

$)\}\delta(\omega - n\Omega)$

$J_n(z')\delta(\omega - n\Omega).$ [18]

line deltas parallel to the k_z axis
ency.
ting transverse magnetization ex-

$C_n(k_z)W(k_z)\}\delta(\omega - n\Omega).$ [19]

$\frac{_1(Az')}{2Az'} * J_n(z')\Big]\delta(\omega - n\Omega),$ [20]

nth sidelobe has the form of a
nverse transform of $W(k_\omega)$ in the
tral islands, Ω, is large compared
ghtforward calculation of M_{xy} for

tion of the Bloch equation in the
2)

$^{z/\Omega)\sin\Omega(t-T)}e^{i\omega(t-T)}dt.$ [21]

$^{in\Omega t}$, [22]

$B_1(t)e^{i(n\Omega+\omega)(t-T)}dt.$ [23]

J_n. This equation can be used to
for most purposes. To approxi-
sum in Eq. [23] can be replaced
of terms required depends upon

To this point we have assumed that the slice-selection gradient varies in a sinusoidal fashion. This is a convenient waveform to generate experimentally, and all of our experiments and simulations have been performed using such a gradient. However, we can also calculate the magnetization resulting when a square-wave gradient is employed. The derivation is similar to that in the sinusoidal case, so we just present the result here.

Assume that $G_z(t)$ is a square wave of amplitude G and period T. The resulting magnetization can then be expressed by

$$M_{xy}(z, \omega) = K_3 M_0(z, \omega)\mathcal{F}^{-1}\{W(k_\omega)\} \times \delta(k_z) ** \sum_{n=-\infty}^{\infty} [\mathcal{F}^{-1}\{W(k_z)\} * a_n(z)]\delta(\omega - n\Omega), \quad [24]$$

where K_3 is a constant and

$$a_n(z) = \begin{cases} \operatorname{sinc}\left(z'' + \frac{n}{2}\right) + \operatorname{sinc}\left(z'' - \frac{n}{2}\right) & \text{for } n \text{ even} \\ \operatorname{sinc}\left(z'' + \frac{n}{2}\right) - \operatorname{sinc}\left(z'' - \frac{n}{2}\right) & \text{for } n \text{ odd.} \end{cases} \quad [25]$$

In this equation $\operatorname{sinc}(x) = (\sin \pi x)/(\pi x)$ and $z'' = (RGT/4\pi)z$.

DESIGN CONSIDERATIONS

We now have expressions for the magnetization excited by a pulse in the presence of an oscillating slice-selection gradient. Using these expressions, we can discuss the design of pulses that are simultaneously selective in space and resonant frequency. Some of the considerations in the design of these pulses are (1) the functional form of the slice-selection gradient, which determines the **k** trajectory, (2) the placement of the desired and undesired components relative to the frequency sidelobes, (3) the amplitude and frequency of the slice-selection gradient, (4) the functional form of the RF envelope, which determines the **k**-space weighting and thus the spatial and spectral slice profiles, (5) the length of the pulse, and (6) the modulation of these pulses to shift them in space and frequency. In this section we discuss these considerations in the context of the design of a water/fat-selective slice-selection pulse.

We wish to design a slice-selective pulse that excites water protons and discriminates against fat protons, or vice versa. The target field strength is 1.5 T, where the difference frequency between water and fat is about 230 Hz. We assume that the main field inhomogeneity across the slice is less than ±1 ppm.

The main requirement for the slice-selection gradient, G_z, is simply that it oscillate in some manner so that the k_ω axis is sampled. Even without referring to **k**-space arguments, it makes intuitive sense that a spatial–spectral pulse would need such a G_z. We know that any long RF pulse will be spectrally selective in the absence of gradients. We want to add a G_z while preserving this spectral selectivity. One way to prevent chemical shift from simply mapping into a shift in the slice-selection direction is to oscillate the gradient. True square-wave gradients are impractical because of slew-rate limitations. Here we choose sinusoidal gradients, which are simple to generate and allow us to verify the theory of the previous section. Trapezoidal gradients are another practical choice.

Before choosing a gradient modulation frequency, we must decide where in the spectrum to place the undesired component, relative to the frequency sidelobes of the excitation pulse. For this discussion, let us assume water is the desired component and fat the undesired component. Water is placed at the central lobe. The simplest method, and the one that we adopt here, is to place fat at the null between the main lobe and the first sidelobe. The required gradient modulation frequency for this method is twice the water/fat difference frequency (460 Hz for 1.5 T). This method leads to the maximum frequency separation between the sidelobes, which has two positive effects: (1) the transition band between water and fat is broad, so that the pulse can be short and (2) the water/fat separation is relatively insensitive to main field inhomogeneity. The main disadvantage of this method is that the minimum slice width is limited, both because the maximum gradient amplitude is limited by slew-rate constraints and because the short gradient period limits the extent of the k_z excursion. If the slice width or slice profile is not acceptable using the above method, then fat can be placed elsewhere (e.g., between the first and second sidelobe) or greater gradient power can be used. It may be advantageous in some circumstances to place fat closer to an odd sidelobe than to an even sidelobe, because the odd symmetry of odd sidelobes results in a decreased integral across the slice.

The placement of fat is strongly influenced by the gradient power and the field strength of the system. When gradient power is sufficiently high, placing fat at the closest null will generally be preferable. For a fixed gradient power, the achievable slice width decreases as the field strength increases. At 1.5 T and using the gradient power available on commercial whole-body imagers, it is possible to achieve slice widths on the order of 1.0 to1.5 cm placing fat at the closest null. This slice width is adequate for many applications. At higher field strengths it may be necessary to place fat elsewhere or to use stronger gradients. At field strengths below 1.0 T placing fat at the closest null should suffice for most applications.

Now that we have chosen the slice-selection gradient as a 460-Hz cosine, we can study the RF envelope. The spatial and spectral weighting can be chosen independently. Here we present a simple pulse with Gaussian weighting on both the k_z and k_ω axes. This weighting leads to compact spectral and spatial slice profiles, which are Gaussian in shape in the small-tip-angle regime. In determining the equations for the pulse, we must choose the value of R, the arbitrary scaling factor for the k_z axis. We want the spatial profile of the main lobe to be as close to the Fourier transform of $W(k_z)$ as possible. It is clear from Eq. [14] with $n = 0$ that we want $A = 1$, because $C_n(k_z)$ would then just be a rectangle function the width of $W(k_z)$. We choose RG to be arbitrarily large relative to one, leading to the expression

$$|\dot{\mathbf{k}}(t)| = \sqrt{\dot{k}_z^2 + \dot{k}_\omega^2} = \sqrt{(RG_z)^2 + 1}$$

$$= \sqrt{[RG\cos\Omega(t-T)]^2 + 1} \qquad [26]$$

$$= RG\cos\Omega(t-T), \quad \text{as} \quad 1/RG \to 0. \qquad [27]$$

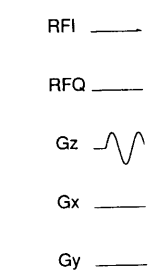

FIG. 2. Rapid gradient–echo pulse seq ing along both k_z and k_ω.

The resulting equations for the p

$$B_1(t) = B_1 e^{-\pi[(\sin}$$

$$G_z(t) = ($$

Figure 2 shows the RF and grad

To achieve more-rectangular axis. For flip angles in the nor weighting can also be determine tion of slice profiles (*23–27*).

With the form of the excitatio U, V, and G remains. T must be tion band is narrower than the bands lead to greater immunity that the RF amplifier can rema phasing and T_2 decay during the isochromat with a frequency off the pulse, assuming that the weig T_2 decay can be thought of as a weighting. We typically choose 13.0 ms. U and V are chosen s without excessive ringing. G is s maximum gradient strength ach a 460-Hz sinusoid, which allows

Now the specifications are co fat, assuming that the transmitte to produce a modulated versio simply multiplies $B_1(t)$ from Eq for a pulse that has been modula

Modulating the pulse to produ cated. To offset the slice by Δz c by approximately 1.5 slice width vious section. Trapezoidal gradi-

:y, we must decide where in the
ve to the frequency sidelobes of
.e water is the desired component
at the central lobe. The simplest
fat at the null between the main
modulation frequency for this
'460 Hz for 1.5 T). This method
·en the sidelobes, which has two
ıter and fat is broad, so that the
ı is relatively insensitive to main
is method is that the minimum
gradient amplitude is limited by
period limits the extent of the k_z
eptable using the above method,
ıe first and second sidelobe) or
ntageous in some circumstances
ı sidelobe, because the odd sym-
l across the slice.
he gradient power and the field
fficiently high, placing fat at the
l gradient power, the achievable
At 1.5 T and using the gradient
rs, it is possible to achieve slice
e closest null. This slice width is
ıgths it may be necessary to place
engths below 1.0 T placing fat at

ient as a 460-Hz cosine, we can
:ighting can be chosen indepen-
an weighting on both the k_z and
d spatial slice profiles, which are
etermining the equations for the
scaling factor for the k_z axis. We
lose to the Fourier transform of
= 0 that we want $A = 1$, because
width of $W(k_z)$. We choose RG
xpression

[26]

$1/RG \rightarrow 0.$ [27]

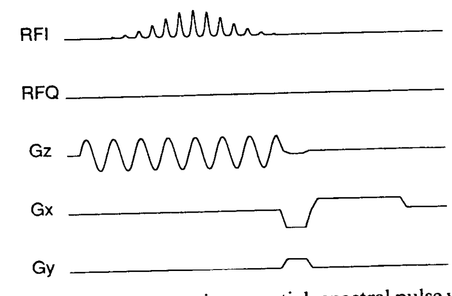

FIG. 2. Rapid gradient–echo pulse sequence using a spatial–spectral pulse with Gaussian k-space weighting along both k_z and k_ω.

The resulting equations for the pulse are

$$B_1(t) = B_1 e^{-\pi[(\sin\Omega(t-T))/U]^2} e^{-\pi[(t-(T/2))/V]^2} \cos \Omega(t-T) \quad [28]$$

$$G_z(t) = G \cos \Omega(t-T), \qquad 0 \leqslant t \leqslant T. \quad [29]$$

Figure 2 shows the RF and gradient waveforms for this pulse.

To achieve more-rectangular pulse profiles, one can use sinc weighting on either axis. For flip angles in the nonlinear regime, the form of the spectral and spatial weighting can also be determined by a 2D extension of 1D techniques for optimization of slice profiles (*23–27*).

With the form of the excitation determined, only the choice of the parameters T, U, V, and G remains. T must be chosen to be long enough so that the spectral transition band is narrower than the water/fat difference frequency. Narrower transition bands lead to greater immunity to main field inhomogeneity. The maximum time that the RF amplifier can remain unblanked sets an upper limit on T. Spectral dephasing and T_2 decay during the pulse also limit T. In the small-tip-angle regime, an isochromat with a frequency offset of $\Delta\omega$ acquires a phase factor of $e^{-i\Delta\omega T/2}$ during the pulse, assuming that the weighting is symmetrical about the midpoint of the pulse. T_2 decay can be thought of as adding the weighting factor $e^{-(T-t)/T_2}$ to the desired weighting. We typically choose T to be equal to six cycles of G_z, which is equal to 13.0 ms. U and V are chosen such that the slice profiles are as narrow as possible without excessive ringing. G is simply chosen to achieve the desired slice width. The maximum gradient strength achievable on our experimental system is 0.7 G/cm for a 460-Hz sinusoid, which allows a minimum slice width of about 1.2 cm.

Now the specifications are complete for a pulse that excites water without exciting fat, assuming that the transmitter is tuned to the water frequency. It is a simple matter to produce a modulated version of this pulse that excites fat instead of water; one simply multiplies $B_1(t)$ from Eq. [28] by $e^{i\Delta\omega t}$. The I- and Q-channel RF waveforms for a pulse that has been modulated by 230 Hz are shown in Fig. 3a.

Modulating the pulse to produce a spatially offset slice is only slightly more complicated. To offset the slice by Δz one multiplies $B_1(t)$ by $e^{ik_z(t)\Delta z}$. A pulse that is offset by approximately 1.5 slice widths is shown in Fig. 3b.

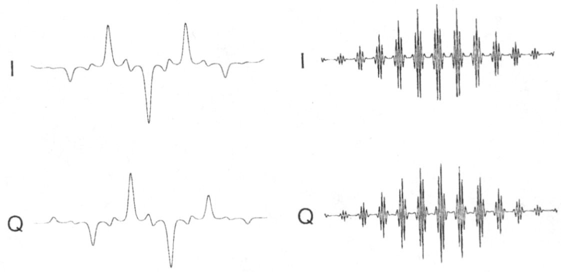

FIG. 3. (a) The I- and Q-channel RF waveforms obtained by modulating the RF waveform of Fig. 2 to shift it 230 Hz along the ω axis. At 1.5 T this pulse will excite fat when the transmitter is tuned to the water frequency. (b) The I- and Q-channel RF waveforms obtained by modulating the RF waveform of Fig. 2 to shift it approximately 1.5 slice widths along the z direction.

SIMULATION RESULTS

In the previous section we discussed a spatially selective pulse designed to selectively excite either water or fat at 1.5 T. In this section we study the behavior of this pulse using a numerical simulation of the Bloch equation. We then compare the simulation results with the results predicted by the small-tip-angle theory. The simulations are performed on the pulse shown in Fig. 2. The object is assumed to be infinite and uniform, and relaxation is neglected.

Figure 4 shows the simulated $|M_{xy}|$ following a 90° pulse as a function of z and ω. The center of the figure corresponds to $z = 0$ and $\omega = 0$. The form of the response agrees well with the small-tip-angle theory. Along the ω axis the islands are spaced at the gradient modulation frequency, Ω. For the central lobe both the spectral and

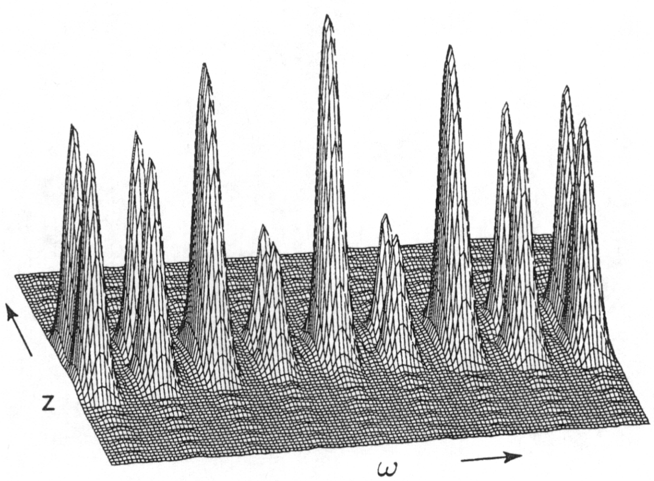

FIG. 4. $|M_{xy}|$ versus z and ω from a computer simulation of the spatial–spectral pulse of Fig. 2 at a flip angle of 90°.

FIG. 5. $|M_{xy}|$ versus z at resonant freq
tion of the spatial–spectral pulse of Fig.
45.5 dB.

spatial slice profiles are Gaussiar
way between the central lobe an
broad null. Figure 5 compares |
nents. The relative suppression
45.5 dB.

In computing the theoretical
contribution from other sidelobe
tion discretely:

$K_2 \mathcal{F}^{-1}$

Figure 6 compares the main-lobe
for 30° and 90° flip angles. The o
pulse was applied along the x axi

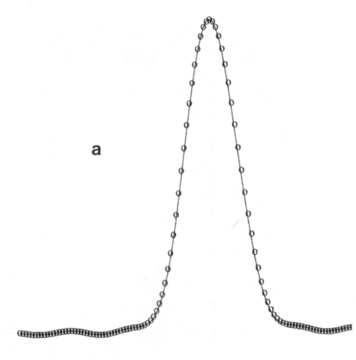

FIG. 6. M_y versus z at two different flip
the theoretical magnetization calculated
simulation of the pulse. (a) M_y versus z a
tip approximation is quite accurate at 30
tion begins to break down at 90°, but the

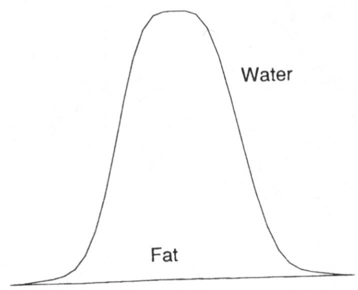

FIG. 5. $|M_{xy}|$ versus z at resonant frequencies corresponding to water and fat from a computer simulation of the spatial–spectral pulse of Fig. 2 at a flip angle of 90°. The suppression of fat relative to water is 45.5 dB.

spatial slice profiles are Gaussian. The undesired component should be placed halfway between the central lobe and the first sidelobe along the ω axis, where there is a broad null. Figure 5 compares $|M_{xy}|$ versus z for the desired and undesired components. The relative suppression for the magnitude of the integral across the slice is 45.5 dB.

In computing the theoretical spatial response at the nth sidelobe, we ignored the contribution from other sidelobes in Eq. [20]. We evaluated the following convolution discretely:

$$K_2 \mathcal{F}^{-1}\{W(k_z)\} * \frac{J_1(Az')}{2Az'} * J_n(z'). \qquad [30]$$

Figure 6 compares the main-lobe theoretical M_y versus z with the simulated response for 30° and 90° flip angles. The only significant magnetization was in M_y, because the pulse was applied along the x axis. The simulated data were corrected for an arbitrary

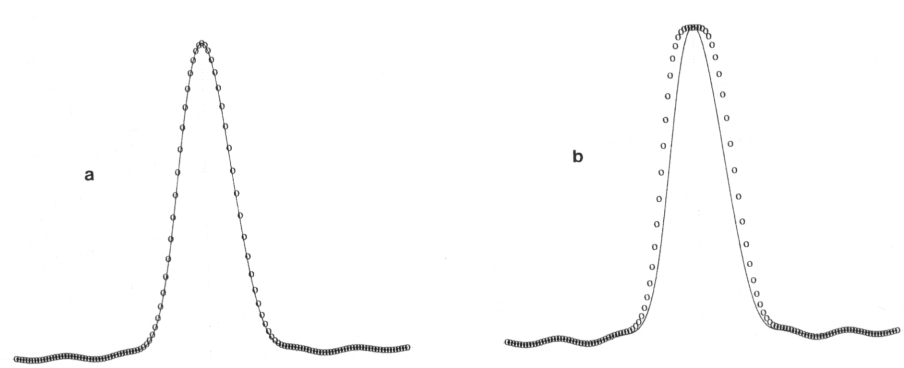

FIG. 6. M_y versus z at two different flip angles for the spatial–spectral pulse of Fig. 2. The solid lines are the theoretical magnetization calculated by discrete convolution. The open circles are from a numerical simulation of the pulse. (a) M_y versus z at a flip angle of 30°. The theoretical expression based on the small-tip approximation is quite accurate at 30°. (b) M_y versus z at a flip angle of 90°. The small-tip approximation begins to break down at 90°, but the slice profile is still quite usable.

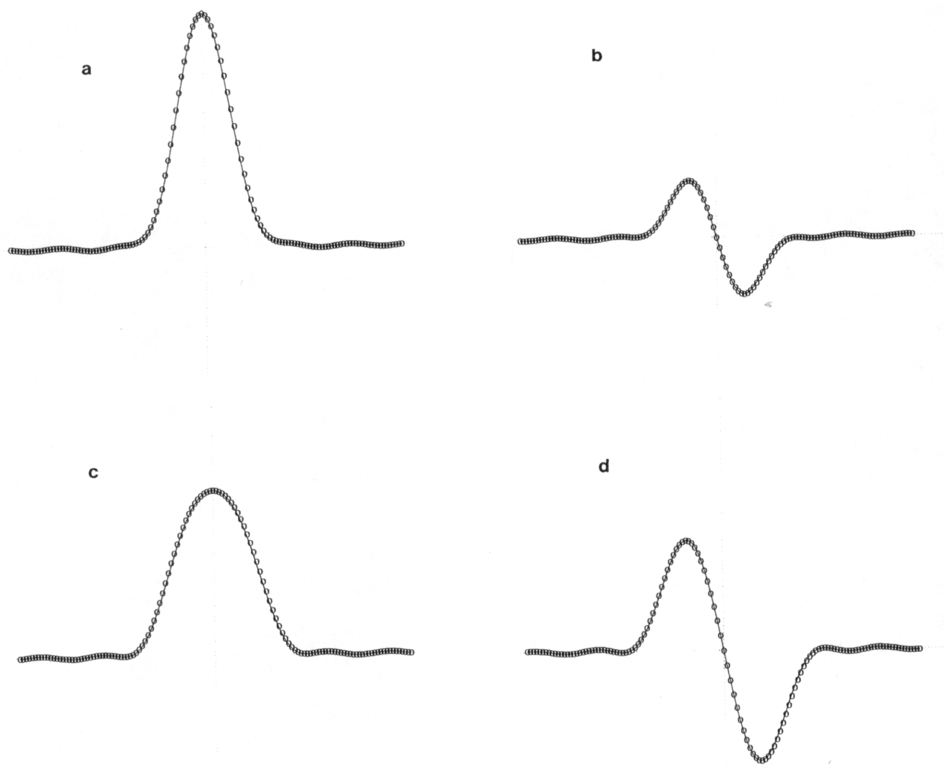

FIG. 7. M_y versus z at 30° for the spatial–spectral pulse of Fig. 2. The magnetization is shown at the center of the main lobe and the first three sidelobes along the ω axis. The solid lines are the theoretical magnetization calculated by discrete convolution. The open circles are from a numerical simulation of the pulse. (a) Main lobe. (b) First sidelobe. (c) Second sidelobe. (d) Third sidelobe.

constant phase factor, but not for any spatially varying phase. The theoretical M_y is almost indistinguishable from the simulated M_y at 30°, which indicates that small-tip-angle approximation is accurate. The response at 90° illustrates that the small-tip-angle approximation is beginning to break down, but the resulting slice profile is actually more rectangular than the 30° profile. This is consistent with current design practice for one-dimensional slice-selection pulses, where useful 90° pulses are often designed by Fourier transform methods, even though the small-tip-angle approximation is not strictly valid at 90°.

Figure 7 compares the theoretical M_y versus z with the 30° simulated response at the main lobe and the first three sidelobes. Once again the agreement is quite good. The even sidelobes have even symmetry and the odd sidelobes have odd symmetry, as predicted.

EXPERIMENTAL RESULTS

The pulse was implemented on a General Electric Signa 1.5-T whole-body imaging system with self-shielded gradient coils. To experimentally verify the sidelobe behav-

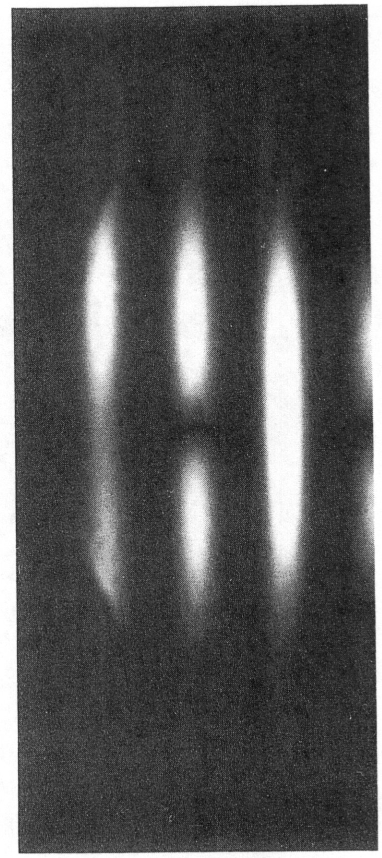

FIG. 8. Experimental $|M_{xy}|$ versus z a
The vertical direction is z, normally th
resonant frequency axis. For this expe
excitation. The sidelobes are truncated a

ior, two gradients were applied
gradient along one direction an
The constant gradient effectivel
tive in the third direction was ap
resulting magnetization. The ob
image is shown in Fig. 8. The re
Fig. 4.

Next the pulse was applied to
water/fat images directly. The w
in Fig. 2. The fat-selective versi
transmitter was tuned to the wa
were alternated with negligible
effective repetition time for wate
the water-selective pulse does n

b

d

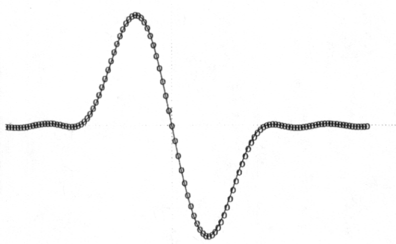

Fig. 2. The magnetization is shown at the
e ω axis. The solid lines are the theoretical
rcles are from a numerical simulation of the
l) Third sidelobe.

ırying phase. The theoretical M_y is
at 30°, which indicates that small-
at 90° illustrates that the small-tip-
ı, but the resulting slice profile is
is is consistent with current design
;, where useful 90° pulses are often
ıgh the small-tip-angle approxima-

with the 30° simulated response at
ıgain the agreement is quite good.
odd sidelobes have odd symmetry,

ULTS

ic Signa 1.5-T whole-body imaging
nentally verify the sidelobe behav-

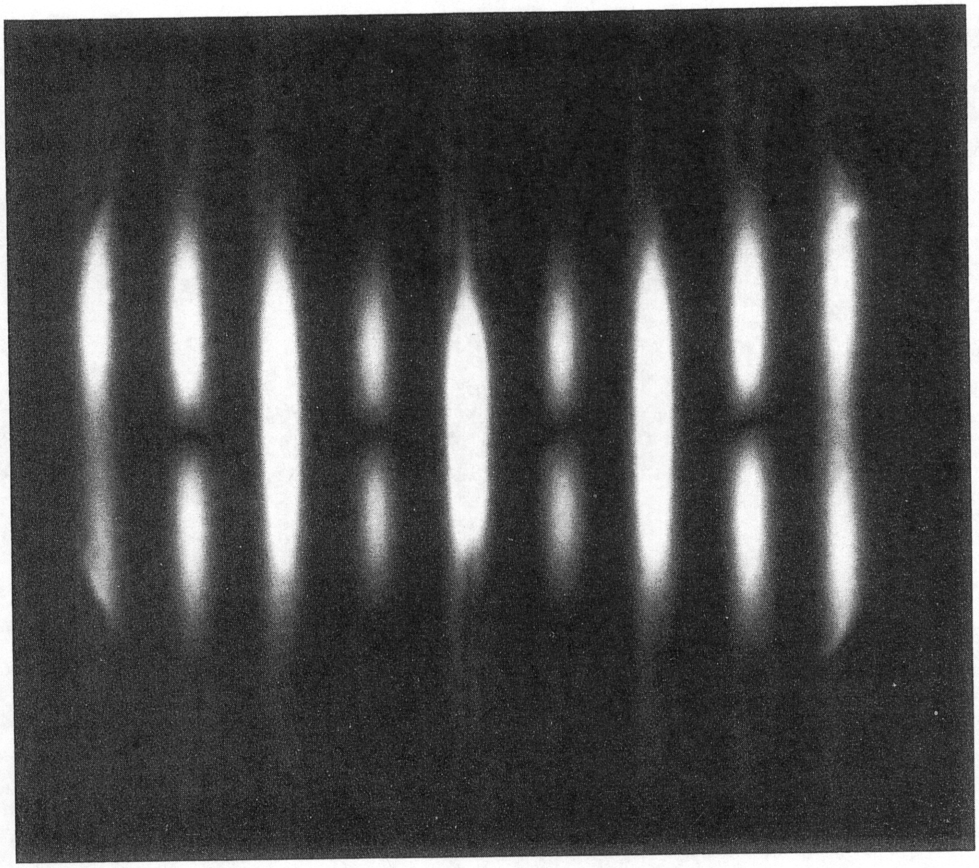

FIG. 8. Experimental $|M_{xy}|$ versus z and ω. This image shows the sidelobes of the spatial–spectral pulse. The vertical direction is z, normally the slice-selection axis. The horizontal direction is ω, normally the resonant frequency axis. For this experiment ω was simulated by applying a constant gradient during excitation. The sidelobes are truncated at the edge of the image by the finite extent of the object.

ior, two gradients were applied during the excitation: the sinusoidal slice-selection gradient along one direction and a constant gradient along an orthogonal direction. The constant gradient effectively simulates a chemical shift axis. A 180° pulse selective in the third direction was applied, and a spin-warp gradient sequence imaged the resulting magnetization. The object was a large sphere of doped water. The resulting image is shown in Fig. 8. The response agrees with the simulated response shown in Fig. 4.

Next the pulse was applied to a rapid gradient–echo imaging sequence to obtain water/fat images directly. The water-selective version of the pulse sequence is shown in Fig. 2. The fat-selective version used the modulated RF pulse of Fig. 3a. The RF transmitter was tuned to the water frequency. The water- and fat-selective versions were alternated with negligible delay between successive sequences. Note that the effective repetition time for water or fat is twice the time between excitations, because the water-selective pulse does not perturb the fat protons and the fat-selective pulse

FIG. 9. Experimental axial head images acquired using the rapid gradient–echo sequence of Fig. 2. The water-selective RF pulse of Fig. 2 was alternated with the fat-selective RF pulse of Fig. 3a so that the effective repetition time of either water or fat was twice the actual repetition time of the transmitter. The total acquisition time for both images was 16 s. (A) Water image: the optic nerves are clearly visible because the orbital fat is suppressed. (B) Fat image.

does not perturb the water protons. By analogy to multislice acquisition mode, we call this multispectrum acquisition mode. With one average, both water and fat images were formed in 16 s. The slice width was approximately 1.2 cm, using a 0.7-G/cm, 460-Hz slice-selection gradient. Figure 9 shows axial images of the head of a normal volunteer obtained with this sequence. The optic nerves are clearly visible in the water image, because the orbital fat is suppressed. The orbital and subcutaneous fat are visible in the fat image. Figure 10 shows axial images of the body of a normal

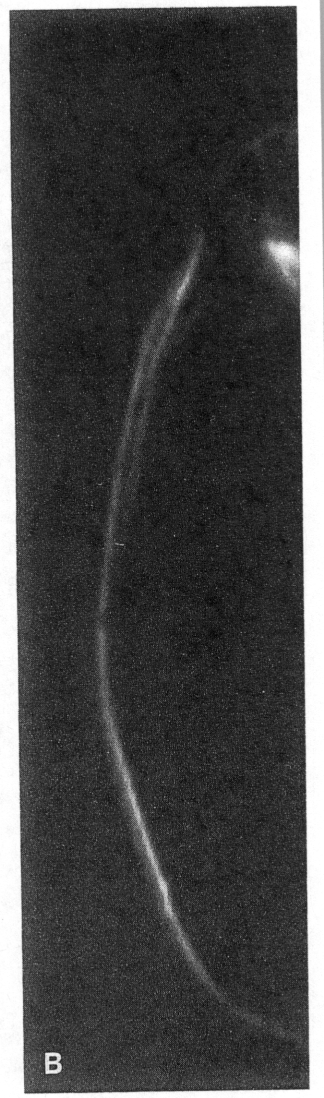

volunteer. Note the absence of
images that are not selective fo
defined and there are no visibl
gradient is well-behaved in th
compensation.

We designed a single pulse tl
We designed this pulse using tl

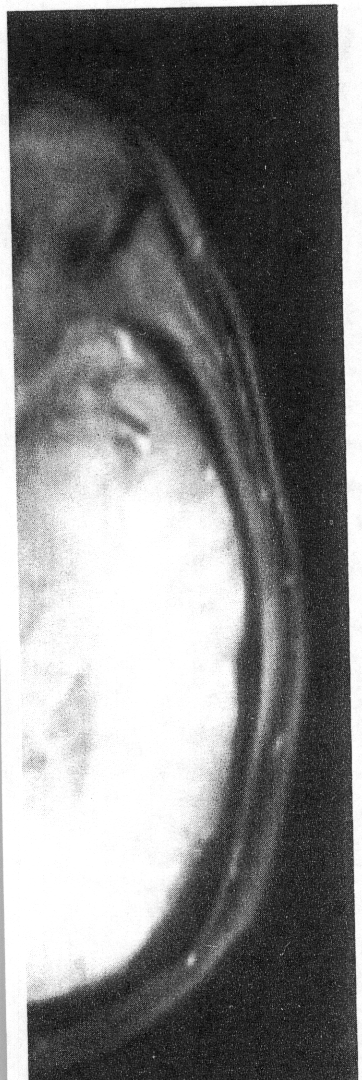

ıpid gradient–echo sequence of Fig. 2. The
t-selective RF pulse of Fig. 3a so that the
ual repetition time of the transmitter. The
:: the optic nerves are clearly visible because

ɔ multislice acquisition mode, we
ıe average, both water and fat im-
roximately 1.2 cm, using a 0.7-G/
ɔws axial images of the head of a
e optic nerves are clearly visible in
ed. The orbital and subcutaneous
ial images of the body of a normal

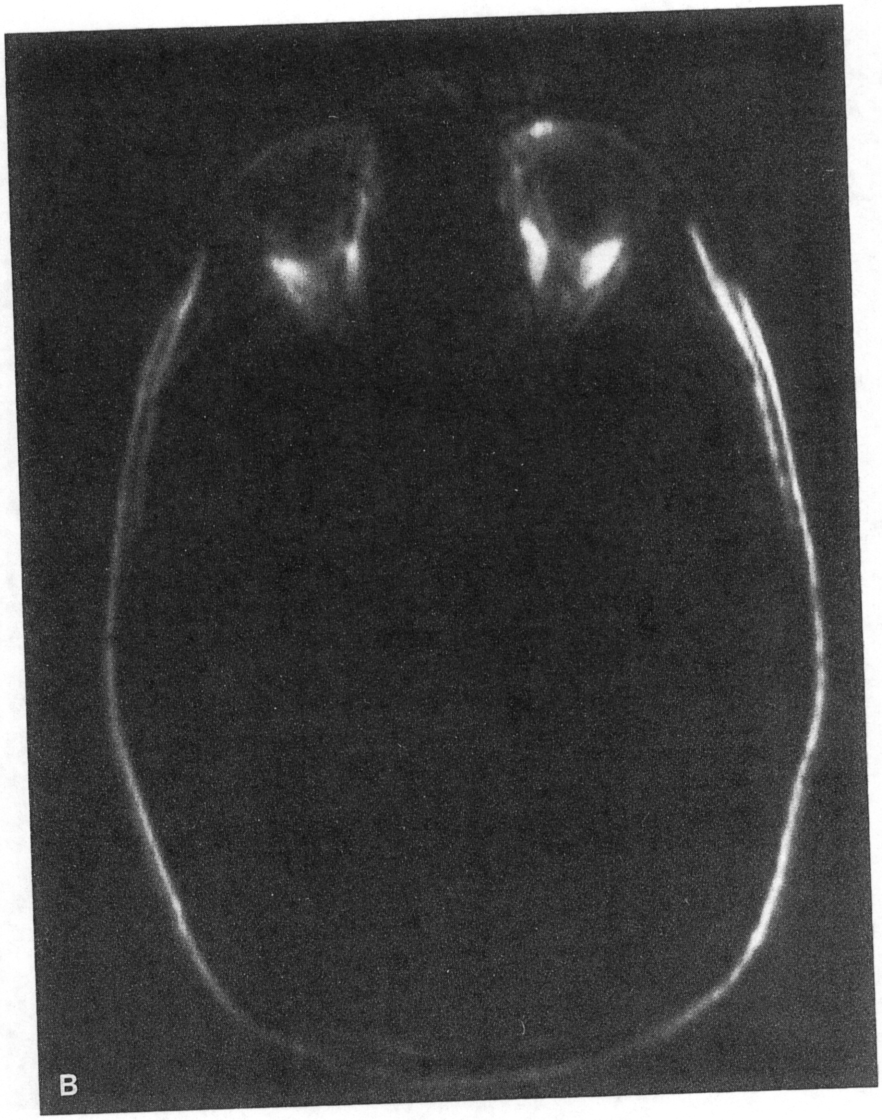

FIG. 9—*Continued*

volunteer. Note the absence of artifacts at the organ boundaries, in contrast to rapid images that are not selective for water or fat. Note also that the blood vessels are well defined and there are no visible flow artifacts. This indicates that the slice-selection gradient is well-behaved in the presence of flow, without any lobes added for flow compensation.

DISCUSSION

We designed a single pulse that is simultaneously spatially and spectrally selective. We designed this pulse using the **k**-space interpretation of small-tip-angle excitation,

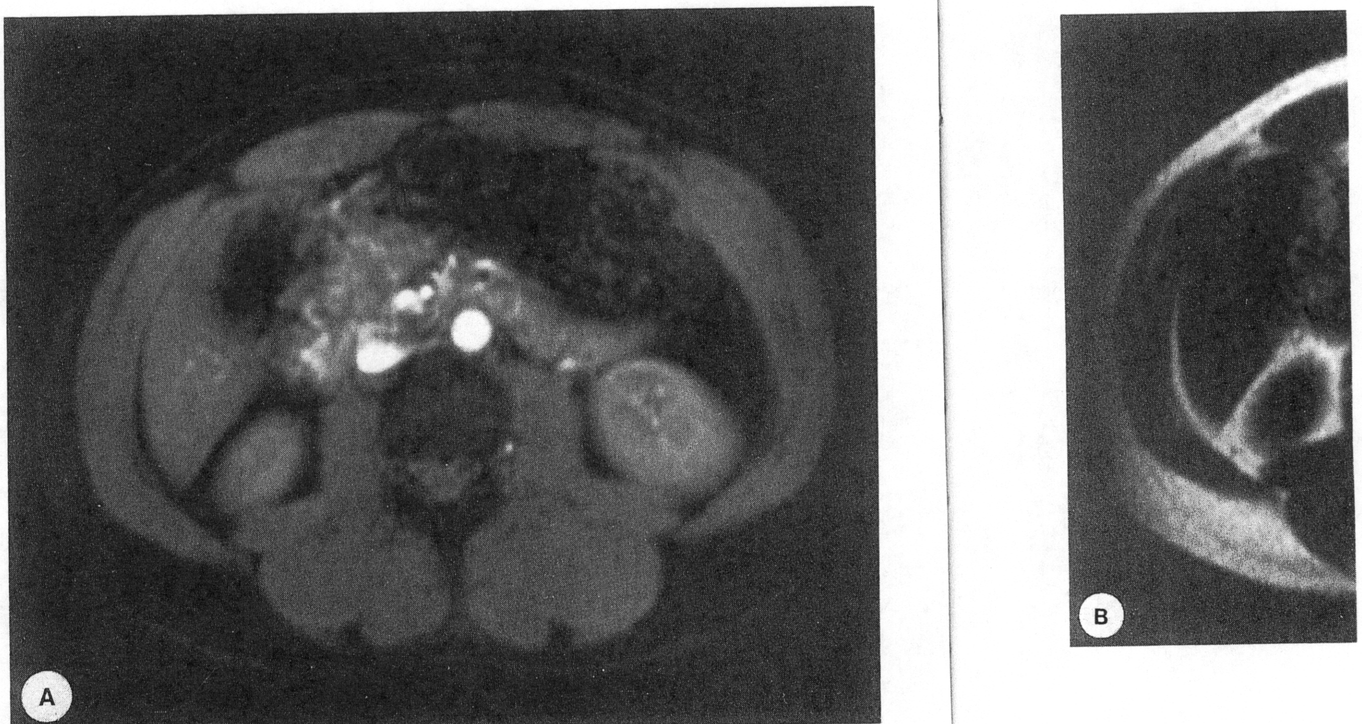

FIG. 10. Experimental axial abdominal images acquired using the same pulse sequence used to acquire Fig. 9. These images have no artifacts at organ boundaries from the interference of water and fat, in contrast to typical rapid gradient–echo images. (A) Water image. (B) Fat image.

an analysis technique developed by Pauly and his co-workers. We derived the inverse Fourier transform of infinite sinusoidal and square-wave line deltas to develop theoretical expressions for the magnetization excited in the presence of an oscillating slice-selection gradient. One useful example of a spatial–spectral pulse is a spatially selective water/fat pulse. We discussed the design of such a pulse for a whole-body 1.5-T imaging system. We presented computer simulations and experimental results and verified that the theoretical expressions are valid. We then applied the pulse to a rapid gradient–echo imaging sequence. The resulting water/fat images are free of the chemical shift artifacts commonly associated with such rapid imaging sequences.

There are a number of advantages of the spatial–spectral pulse. We have shown experimentally that it is useful in rapid gradient–echo imaging sequences, particularly in the abdomen. Problems with interference between water and fat at organ boundaries disappear. Because only one spectral element is excited at a time, multispectrum imaging is possible, as demonstrated by the alternation of the water and fat excitations in the gradient–echo sequence. The moments of the slice-selection gradient are small, so flow artifacts are minimized. At the end of pulse the magnetization is inherently refocused and the short refocusing interval is only necessary because of the finite gradient switching time. There is no misregistration in the z direction between the water and fat slices. Unlike water/fat sequences with one spatially selective pulse and

a separate spectrally selective pu
mode. This pulse is unique in it
the same set of spatial slices; the
rely on the spatial misregistratio
multislice and multispectrum ex
spectral component in sequence

There are of course some pract
suppression that can be achieve
a system is the primary limit. S
the pulse somewhat more difficu
currents, a phase shift of the slic
The length of the pulse is limite
that the RF amplifier can remai
tion may be impractical for extr

This pulse is especially useful
planar imaging or square-spiral
make water/fat excitation a nec
cardiac movies, where the seque
eral times during a heartbeat. Th
cardiac movies, because it suppr
dephase the flowing blood. We h
imaging, both to form water-sel

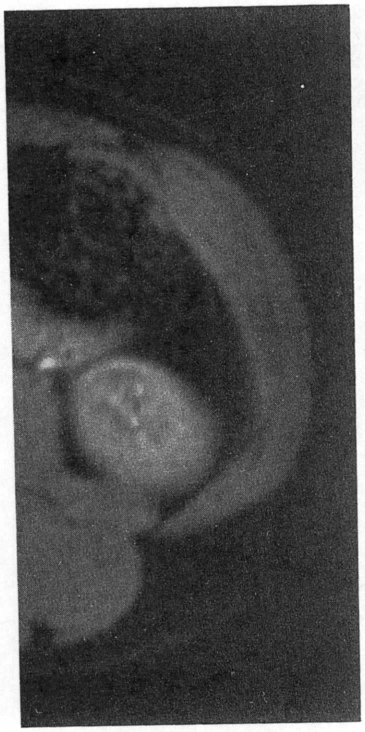

ɩg the same pulse sequence used to acquire
:he interference of water and fat, in contrast
ɩt image.

o-workers. We derived the inverse
:-wave line deltas to develop theo-
the presence of an oscillating slice-
–spectral pulse is a spatially selec-
ch a pulse for a whole-body 1.5-T
ons and experimental results and
. We then applied the pulse to a
ng water / fat images are free of the
such rapid imaging sequences.
ɩl–spectral pulse. We have shown
ɩo imaging sequences, particularly
:en water and fat at organ bound-
s excited at a time, multispectrum
ion of the water and fat excitations
: slice-selection gradient are small,
ɩe the magnetization is inherently
y necessary because of the finite
ɔn in the z direction between the
h one spatially selective pulse and

FIG. 10—*Continued*

a separate spectrally selective pulse, this pulse can be used in a multislice acquisition mode. This pulse is unique in its ability to perform multislice water / fat imaging of the same set of spatial slices; the other published multislice water / fat pulse sequences rely on the spatial misregistration of water and fat. One can even perform a combined multislice and multispectrum experiment, where one excites each desired spatial and spectral component in sequence.

There are of course some practical limits to the slice width, slice profile, and spectral suppression that can be achieved with this pulse. The gradient slew rate available on a system is the primary limit. Severe eddy currents might make implementation of the pulse somewhat more difficult on some systems, but the main effect of such eddy currents, a phase shift of the slice-selection gradient, can easily be compensated for. The length of the pulse is limited by T_2 decay and by the maximum length of time that the RF amplifier can remain unblanked. Finally, any water / fat-selective excitation may be impractical for extremely low-field systems, because $\Delta\omega$ is too small.

This pulse is especially useful in rapid **k**-space scanning sequences such as echo planar imaging or square-spiral imaging. In such sequences the long readout times make water / fat excitation a necessity. One common use of these sequences is to form cardiac movies, where the sequence is repeated, with small-tip-angle excitations, several times during a heartbeat. The spatial–spectral pulse is particularly useful in these cardiac movies, because it suppresses fat without a 180° pulse and because it does not dephase the flowing blood. We have applied the spatial–spectral pulse to square-spiral imaging, both to form water-selective cardiac movies and to form water / fat multislice fast images of the heart and the abdomen (*15*). We will report further on this work in a later paper.

ACKNOWLEDGMENTS

The authors gratefully acknowledge the support of the GE Medical Systems Group under Grant 22-84 and the National Institutes of Health under Grant 1R01 HL-39297.

REFERENCES

1. A HAASE, J. FRAHM, D. MATTHAEI, W. HÄNICKE, AND K. MERBOLDT, *J. Magn. Reson.* **67,** 258 (1986).
2. F. W. WEHRLI, "Introduction to Fast-Scan Magnetic Resonance," General Electric Medical Systems, 1985.
3. P. VAN DER MEULEN, J. P. GROEN, AND J. J. M. CUPPEN, *Magn. Reson. Imaging* **3,** 297 (1985).
4. M. L. GYNGELL, *Magn. Reson. Imaging* **6,** 415 (1988).
5. R. C. HAWKES AND S. PATZ, *Magn. Reson. Med.* **4,** 9 (1987).
6. R. R. RZEDZIAN, *in* "Proceedings, Sixth Annual Meeting of the Society of Magnetic Resonance in Medicine," p. 229, 1987.
7. C. H. MEYER AND A. MACOVSKI, *in* "Proceedings, Sixth Annual Meeting of the Society of Magnetic Resonance in Medicine," p. 230, 1987.
8. R. COXON, R. J. ORDRIDGE, B. CHAPMAN, AND P. MANSFIELD, *in* "Proceedings, Seventh Annual Meeting of the Society of Magnetic Resonance in Medicine," p. 242, 1988.
9. P. M. JOSEPH, *J. Comput. Assist. Tomogr.* **9**(4), 651 (1985).
10. C. L. DUMOULIN, *Magn. Reson. Med.* **2,** 583 (1985).
11. A. VOLK, B. TIFFON, J. MISPELTER, AND J. LHOSTE, *J. Magn. Reson.* **71,** 168 (1987).
12. H. W. PARK, D. J. KIM, AND Z. H. CHO, *Magn. Reson. Med.* **4,** 526 (1987).
13. J. PAULY, D. NISHIMURA, AND A. MACOVSKI, *J. Magn. Reson.* **81,** 43 (1989).
14. C. H. MEYER, J. M. PAULY, A. MACOVSKI, AND D. G. NISHIMURA, *in* "Abstract Book, Second European Congress of NMR in Medicine and Biology," p. 14, 1988.
15. C. H. MEYER, J. M. PAULY, A. MACOVSKI, AND D. G. NISHIMURA, *in* "Proceedings, Seventh Annual Meeting of the Society of Magnetic Resonance in Medicine," p. 653, 1988.
16. T. R. BROWN, B. M. KINCAID, AND K. UGURBIL, *Proc. Nat. Acad. Sci. USA* **79,** 3523 (1982).
17. S. LJUNGGREN, *J. Magn. Reson.* **54,** 338 (1983).
18. D. B. TWIEG, *Med. Phys.* **10,** 610 (1983).
19. R. S. LIKES, U.S. Patent 4,307,343, 1981.
20. P. MANSFIELD AND P. MORRIS, "NMR Imaging in Biomedicine," Academic Press, New York, 1982.
21. A. PAPOULIS, "Systems and Transforms with Applications in Optics," McGraw–Hill, New York, 1968.
22. I. SHENBERG, "Magnetic Resonance Imaging with Time-Varying Gradients," Ph.D. thesis, Stanford University, 1986.
23. S. M. CONOLLY, D. G. NISHIMURA, AND A. MACOVSKI, *IEEE Trans. Med. Imaging* **MI-5,** 106 (1986).
24. J. B. MURDOCH, A. H. LENT, AND M. R. KRITZER, *J. Magn. Reson.* **74,** 226 (1987).
25. M. SHINNAR, L. BOLINGER, AND J. S. LEIGH, *in* "Proceedings, Seventh Annual Meeting of the Society of Magnetic Resonance in Medicine," p. 659, 1988.
26. P. LE ROUX, *in* "Proceedings, Seventh Annual Meeting of the Society of Magnetic Resonance in Medicine," p. 1049, 1988.
27. J. PAULY, D. NISHIMURA, AND A. MACOVSKI, *in* "Proceedings, Eighth Annual Meeting of the Society of Magnetic Resonance in Medicine," p. 862, 1989.

Improved Quantification of
of Signal Acquisition
# of Prior Know

A. A. DE G

Department of Appl
P.O. Box 50

Quantification of localized *in*
excessive spectral overlap. In ac
of the NMR pulse sequence on
these problems. It comprises opt
mental lineshape; determinatior
linewidths using model solutior
edge into a nonlinear least-squa
greatly improved accuracy, pre
spectra of rat brain, and enabl

To study the pathology of hep
and phosphorus *in vivo* NMR sp
determination of small concentr
spectral quantification is essentia
mination of peak heights or of pe
ing excised peaks are not able t
fitting the spectrum or the time c
domain fitting by the LPSVD me
(*4*), but for ^{1}H MRS some prol
lineshapes, the residual water si
water suppression pulse sequenc
ress is made in solving these pro
spectral region of interest. This h
(*7*). The following special proble

1. Fitting in the frequency do
2. The signal-to-noise ratio (S
3. The experimental lineshap
tions (Lorentzian and/or Gauss
mogeneity, motions of the anim
4. In the case of strong overl
ances of the fitting results will b
tween the fitted parameters.